MARS

Long-term drying of Mars by sequestration of ocean-scale volumes of water in the crust

E. L. Scheller[1]*, B. L. Ehlmann[1,2], Renyu Hu[2], D. J. Adams[1], Y. L. Yung[1,2]

Geological evidence shows that ancient Mars had large volumes of liquid water. Models of past hydrogen escape to space, calibrated with observations of the current escape rate, cannot explain the present-day deuterium-to-hydrogen isotope ratio (D/H). We simulated volcanic degassing, atmospheric escape, and crustal hydration on Mars, incorporating observational constraints from spacecraft, rovers, and meteorites. We found that ancient water volumes equivalent to a 100 to 1500 meter global layer are simultaneously compatible with the geological evidence, loss rate estimates, and D/H measurements. In our model, the volume of water participating in the hydrological cycle decreased by 40 to 95% over the Noachian period (~3.7 billion to 4.1 billion years ago), reaching present-day values by ~3.0 billion years ago. Between 30 and 99% of martian water was sequestered through crustal hydration, demonstrating that irreversible chemical weathering can increase the aridity of terrestrial planets.

There is abundant geomorphological evidence for large volumes of surface liquid water early in martian history (*1*), with estimated volumes equivalent to a ~100 to 1500 m global equivalent layer (GEL) (*1–4*). Liquid water on Mars decreased over geological time; presently, most water is stored in the polar ice caps or as subsurface ice. Estimates for the total modern water inventory, in the atmosphere and as ice, total a 20 to 40 m GEL (*5–8*). The availability of water to participate in the hydrologic cycles of terrestrial planets is expected to influence their climate and habitability. However, the processes that caused the decline of available water on Mars are poorly constrained.

Previous studies have suggested that Mars experienced substantial water loss from atmospheric escape, which is supported by the current atmospheric deuterium-to-hydrogen isotope ratio (D/H) of 5 to 10 × SMOW (standard mean ocean water on Earth; D/H at 1 SMOW is 155.76×10^{-6}) (*5, 9–11*). The D/H value at ~4 billion years ago was 2 to 4 × SMOW, inferred from martian meteorites (fig. S1) (*12, 13*). Existing models used these observations, combined with assumed atmospheric escape fractionation factors (α_{escape}) of 0.016 to 0.32 during loss, to estimate integrated atmospheric escape of at least 10 to 200 m GEL (fig. S1) (*4, 5, 11, 14, 15*). These estimates imply an initial 50 to 240 m GEL of water on ancient Mars, which is consistent only with the lower range of geological estimates (100 to 1500 m GEL) (*1–4*). This has been interpreted as implying a large, unknown reservoir of water on present-day Mars (*4*).

For present-day Mars, the rate of atmospheric water loss is measured from the H escape flux

because water vapor dissociates in the atmosphere and its hydrogen escapes. Spacecraft measurements of the current H escape flux, 10^{26} to 10^{27} H atoms s^{-1}, are equivalent to the escape of 3 to 25 m GEL water across 4.5 billion years (*16, 17*) and cannot explain all the water loss. Another potential water loss mechanism is crustal hydration through irreversible chemical weathering, in which

water and/or hydroxyl are incorporated into minerals. Orbital and in situ data show that widespread chemical weathering has produced a substantial reservoir of hydrous minerals on Mars, potentially totaling hundreds of meters of GEL in the crust (*5, 18*). We hypothesized that crustal hydration during the first 1 billion to 2 billion years decreased the volume of the hydrologically available water reservoir, followed by subsequent atmospheric loss that fractionated the martian atmosphere to its current observed D/H. We simulated water loss through geological time to constrain Mars' water history and to compare the simulations to D/H data from the Curiosity rover (*5*) and laboratory analyses of martian meteorites (fig. S1) (*12, 13, 19–21*).

A hydrogen isotope water reservoir model

We developed a water budget and D/H model that integrates water sinks and sources, including crustal hydration, volcanic degassing, and atmospheric escape (Fig. 1) (*5*). Most previous models included only atmospheric escape (*4, 11, 14*); one model (*15*) also included volcanic degassing. We treat liquid water, ice, and atmospheric vapor as a single exchangeable reservoir, an isotopic modeling technique that was originally developed for carbon
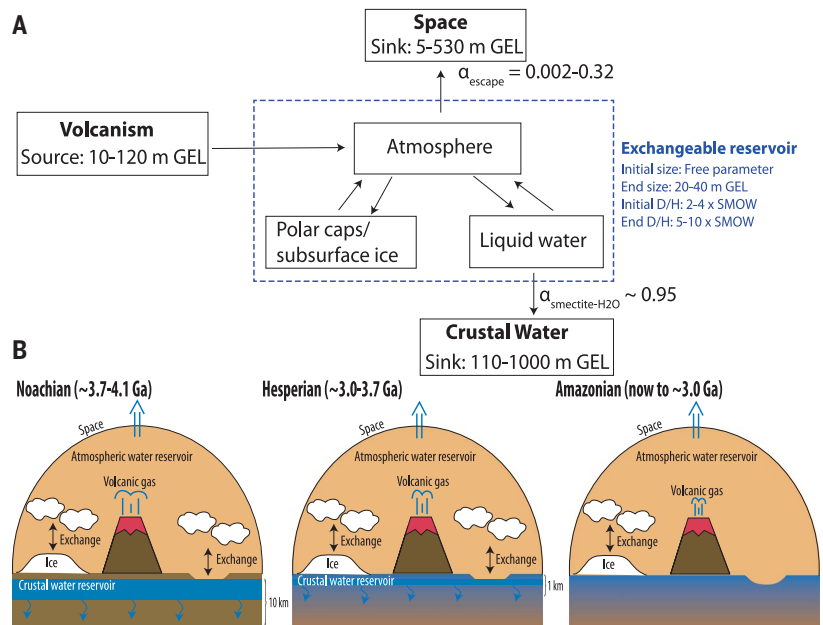

Fig. 1. Schematic illustration of water sink and source fluxes considered in our simulations. (**A**) Box model representation with ranges of integrated water sinks, sources, reservoir sizes, and fractionation factors adopted in our simulations. The crustal water reservoir is based on rover and remote sensing observations and represents all unexchangeable subsurface ice, liquid water, and structural water in minerals (*5*). The integrated amount of H escape to space is based on measurements of the current flux and KINETICS calculations of fluxes (figs. S2 and S3). The integrated volcanic degassing is based on thermochemical models (*5, 24*). The blue box indicates the exchangeable reservoir, with its properties in blue text. (**B**) Schematic representation of our assumptions for the Noachian, Hesperian, and Amazonian periods. During the Noachian, the fluxes associated with crustal hydration and volcanic degassing are high. These all reduce during the Hesperian. During the Amazonian, volcanic degassing falls further, and there is negligible crustal hydration because the water is predominantly solid ice. Ga, billion years ago.

[1]Division of Geological and Planetary Sciences, California Institute of Technology, Pasadena, CA 91125, USA. [2]Jet Propulsion Laboratory, California Institute of Technology, Pasadena, CA 91109, USA.
*Corresponding author. Email: eschelle@caltech.edu

reservoir models (22). We assume that liquid and solid phases, not vapor, dominate the exchangeable reservoir and that fractionation between them is negligible [the fractionation factor is $\alpha_{ice-liquid} = 1.02$ (23)]. Our simulations are constrained so that the exchangeable reservoir can never be negative and must reproduce 20 to 40 m GEL water today. The initial exchangeable reservoir size ($X_{ex,0}$)—the ancient hydrologically available water inventory—is a free parameter except during sensitivity analyses. We determined permitted ranges of source and sink fluxes for crustal hydration (F_{crust}), volcanic degassing ($F_{volcanic}$), and atmospheric escape (F_{esc}) during the Noachian (~4.0 billion to 3.7 billion years ago), Hesperian (~3.7 billion to 3.0 billion years ago), and Amazonian (~3.0 billion years ago to present) periods of martian geological history following observational and previous model constraints (Fig. 1 and table S1) (5). Models were evaluated by their ability to reproduce the D/H of the present-day exchangeable reservoir ($R_{ex,end}$) of 5 to 10 × SMOW. We also compared our simulation results with a compilation of Curiosity rover Sample Analysis at Mars (SAM) data sets that recorded a D/H composition range of 3 to 5 × SMOW for gas released from Hesperian samples during high-temperature (>374°C) combustion experiments (5).

We calculated a permitted range of F_{crust} from measurements of water wt % in Mars surface materials and global remote sensing observations of hydrated minerals. The mass fraction of crustal water is based on rover measurements from Gale crater, orbital global infrared and neutron spectrometer data, and measurements of the NWA 7034 martian meteorite (0.5 to 3 wt % water) (5). The volume of the crustal reservoir is based on orbital measurements of clay exposure depths in the Valles Marineris canyon and craters 5 to 10 km in depth (5, 18). We adopted permitted ranges of 100 to 900 m GEL of water in Noachian-aged crust and 10 to 100 m GEL of water in Hesperian-aged crust on the basis of this analysis (table S1) (5, 18). Although F_{crust} is based on observations of hydrated minerals, we considered crustal water as a single reservoir representing any combination of ice, liquid, and structural water, formerly participating in the hydrologic cycle, that now no longer exchange isotopes with the exchangeable reservoir. We determined $F_{volcanic}$ using previous thermochemical models of the martian mantle (24). Different parameterizations of those models (24) predict outgassing of a 10 to 120 m GEL of water from volcanic processes since 4.1 billion years ago (5, 24). We considered Noachian and Hesperian F_{esc} values between 10^{25} and 10^{30} H atoms s^{-1} and adopted the measured current escape rate of 5 × 10^{26} H atoms s^{-1} for the Amazonian (table S1) (5). We compared these escape fluxes with simulations
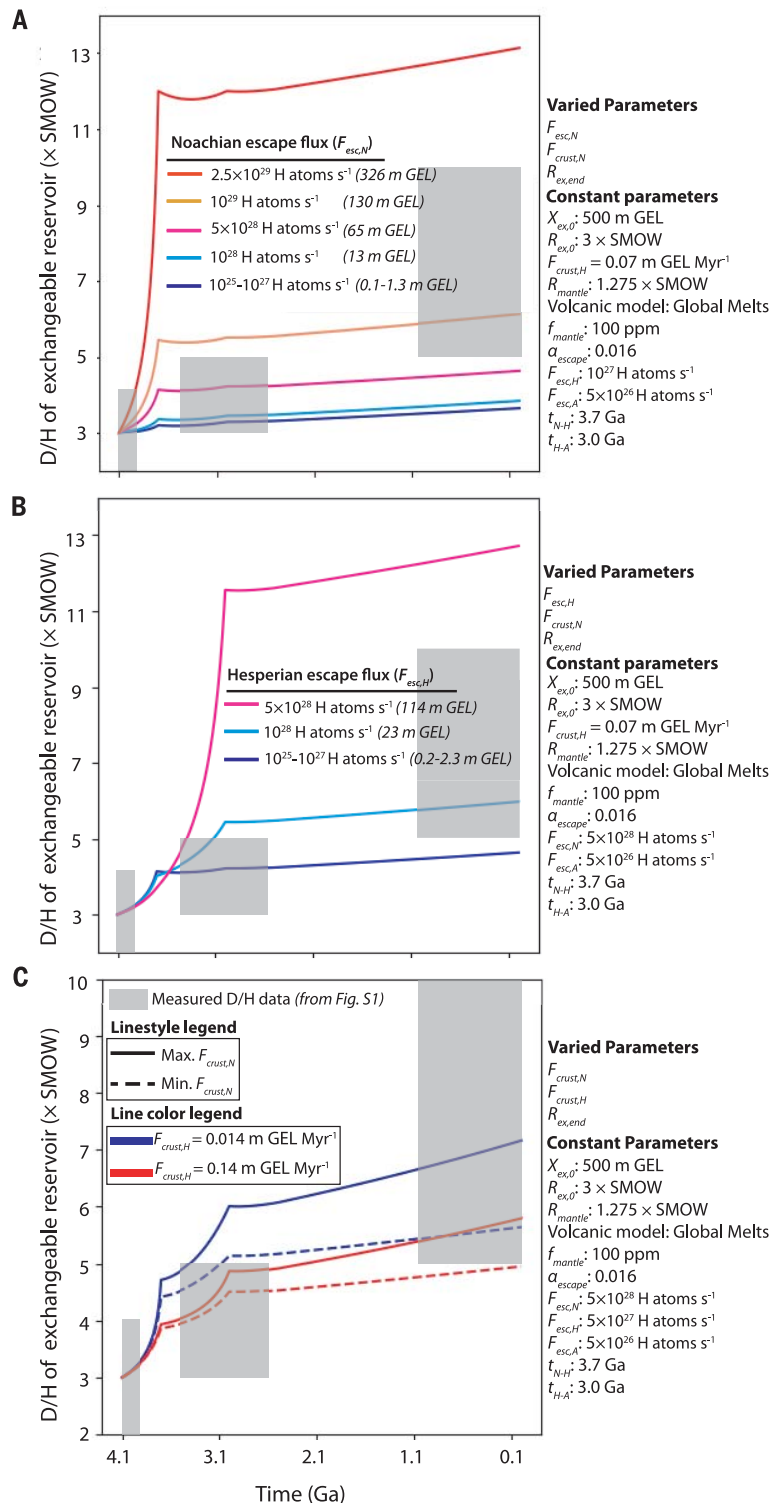

Fig. 2. Simulated D/H evolution for different assumptions of crustal hydration and atmospheric escape rates. (**A** to **C**) The evolution of the D/H of the exchangeable reservoir in our simulation. Most parameters, including $X_{ex,0}$, are fixed; $R_{ex,end}$ is a free parameter to visualize the model sensitivity. The colored lines show results for different assumptions of the flux rates. The large range of D/H measurements from meteorite, rover, and telescope observations are indicated with gray rectangles (fig. S1). (A) Effects of increasing the Noachian escape flux ($F_{esc,N}$). (B) Effects of increasing the Hesperian escape flux ($F_{esc,H}$). (C) Effects of increasing the Noachian ($F_{crust,N}$) and Hesperian ($F_{crust,H}$) crustal hydration fluxes. When $F_{crust,N}$ increases, the exchangeable reservoir becomes smaller, inducing larger fractionations during the Noachian. When $F_{crust,H}$ increases, the allowed values of $F_{crust,N}$ decrease, causing less fractionation during the Noachian.
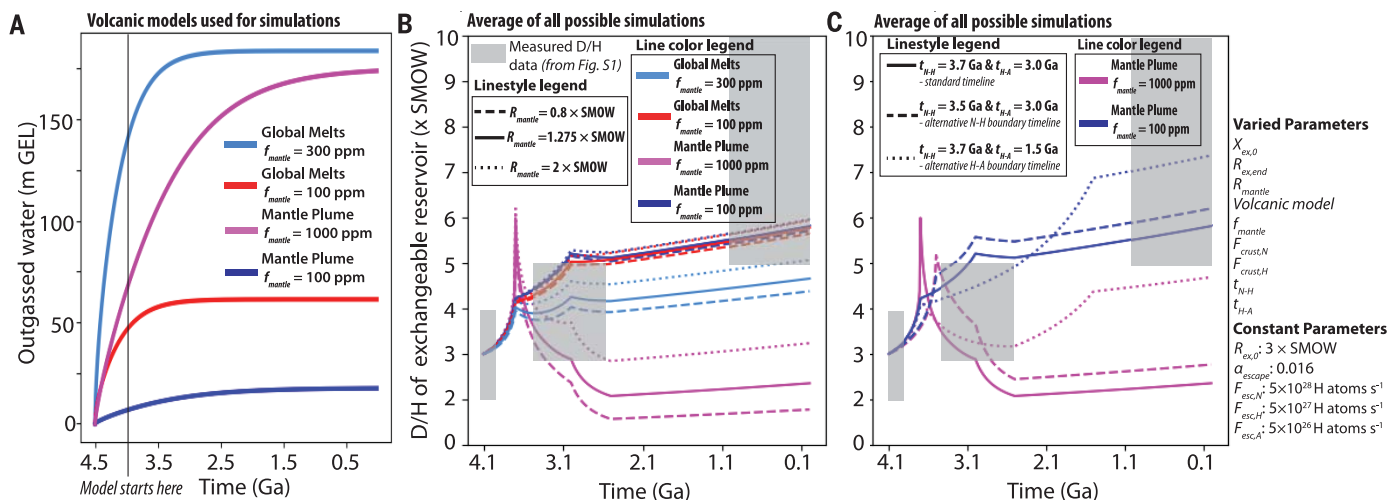
Fig. 3. Simulated D/H evolution for different assumptions of the volcanic outgassing as a function of time. (**A**) Adopted volcanic models (5, 24). The Mantle Plume model (24) assumes an initial mantle water content (f_{mantle}) of 100 ppm (dark blue) or 1000 ppm (purple). The alternative Global Melts model (24) assumes f_{mantle} is 100 ppm (red) or 300 ppm (light blue). (**B**) The evolution of the D/H ratio in the exchangeable reservoir from an average of simulations with each assumed volcanic model. Line colors are the same as in (A), and gray boxes are the same as in Fig. 2. Line styles refer to assumed D/H composition of volcanic gas [dashed, 0.8 × SMOW (27); solid, 1.275 × SMOW (47); and dotted, 2 × SMOW (19)]. (**C**) Evolution of the D/H in the exchangeable reservoir for average of simulations with different assumptions of volcanic model and age of the Noachian-Hesperian boundary (t_{N-H}) and the Hesperian-Amazonian boundary (t_{H-A}) (5). These transition ages control when F_{esc} and F_{crust} values change under our assumptions for the Noachian, Hesperian, and Amazonian periods (5). Line colors are the same as in (A). Line styles refer to the assumed timing of t_{N-H} and t_{H-A} (solid, standard boundary ages where t_{N-H} is 3.7 Ga and t_{H-A} is 3.0 Ga; dashed, t_{N-H} is moved to 3.5 Ga; dotted, t_{H-A} is moved to 1.5 Ga). In these simulations, $R_{ex,end}$ is allowed to vary.

using the one-dimensional (1D) photochemical model KINETICS (25, 26) with adopted past solar extreme ultraviolet flux, variable atmospheric pressures, and mesospheric and surface temperatures (table S2) (5).

Controls on D/H and water loss

In our model, stepwise mixing between the exchangeable reservoir and the depleted volcanically outgassed water vapor (0.8 to 2 × SMOW) (fig. S1 and table S1) (5, 19, 27) causes the D/H of the exchangeable reservoir to decrease (5). We do not include fractionation associated with degassing or its redox sensitivity because these are negligible compared with the large range of potential D/H compositions of the volcanic gas inferred from meteorites (5). Atmospheric escape causes D/H of the exchangeable reservoir to fractionate toward heavier values, which we modeled through stepwise Rayleigh distillation, a common isotopic reservoir modeling technique, at each 10-million-year time step with an α_{escape} of 0.002 to 0.32 (28–30). The fractionation factor between smectite, the most common hydrated mineral found on Mars, and water [$\alpha_{smectite-H_2O} = 0.95$ (5)] is used in the stepwise Rayleigh distillation model as a first-order approximation of fractionation through crustal hydration (table S3) (5); we found that this fractionation is minor compared with that caused by atmospheric escape.

The D/H of the exchangeable reservoir increases during the Noachian in all our simu-

lations, and through the Hesperian in most of them, because of a combination of crustal hydration and atmospheric escape (Figs. 2 and 3). Higher $F_{esc,N}$ and $F_{esc,H}$ increase D/H fractionations of the exchangeable reservoirs (Fig. 2, A and B). We found that the Noachian and Hesperian H escape flux ranges that satisfy the model constraints (fig. S2) have a wide allowable range, ~0.1 to 1000 times the current 5 × 10^{26} H atoms s^{-1} escape flux. Independently, our KINETICS photochemical simulations (5) produced the same range (~10^{25} to 5 × 10^{29} H atoms s^{-1}) (fig. S3). We considered multiple scenarios, including (i) a range of standard ancient Mars conditions, (ii) high-altitude water injection [60 parts per million (ppm) at 100 km], and (iii) fixing a surface H_2 mixing ratio of 10^{-3}, which is higher than present-day levels of 10^{-5} (26). The maximum KINETICS-permitted escape flux (~5 × 10^{29} H atoms s^{-1}) and our D/H model maximum permitted flux (4 × 10^{29} H atoms s^{-1}) match the diffusion-limited escape of 5 × 10^{29} H atoms s^{-1} that we calculated using equations from (31). The injection of high-altitude water and increased surface H_2 concentrations both increase the production of high-altitude H_2; one or both would be required for loss fluxes 100 to 1000 times higher than that of the present (fig. S3).

Crustal hydration during early Mars history also increases D/H fractionation of the exchangeable reservoirs, with the permitted range of $F_{crust,N}$ depending on the assumed $F_{crust,H}$ (Fig. 2C). This is primarily because

higher $F_{crust,N}$ decreases the exchangeable reservoir size, not because of the fractionation [$\alpha_{smectite-H_2O} = 0.95$ (5)] associated with clay formation. Because the exchangeable reservoir is reduced through crustal hydration, less atmospheric escape is needed to produce the modern D/H of the atmosphere. During the Noachian, decreasing exchangeable reservoir size and increasing D/H are a feature of all of our simulations. Changes to the assumed timing of the boundary between the Noachian and Hesperian (t_{N-H}) and balance of $F_{crust,N}$ to $F_{crust,H}$ only slightly affect the Noachian D/H fractionation (Figs. 2C and 3C). During the Amazonian, the exchangeable reservoir size is low, and its D/H increases slightly in all our simulations because of the lack of crustal hydration, low H escape flux (assumed equal to the present rate), and a low volcanic degassing flux (Figs. 2 and 3). By contrast, the D/H evolution during the Hesperian is less well constrained because models with low total volcanic outgassing (10 to 20 m GEL) result in D/H increases, whereas models with high outgassing (60 to 120 m GEL) result in D/H decreasing or staying approximately constant (Fig. 3, A and B). The amount of volcanic degassing controls the required sizes of F_{crust} and F_{esc} for different $X_{ex,0}$ to reproduce the present-day D/H ($R_{ex,end}$) (figs. S4 to S6). Evolution of Hesperian D/H is also sensitive to the absolute timing of the debated (5) boundary between the Hesperian and Amazonian periods (t_{H-A}) because in our model, that boundary sets
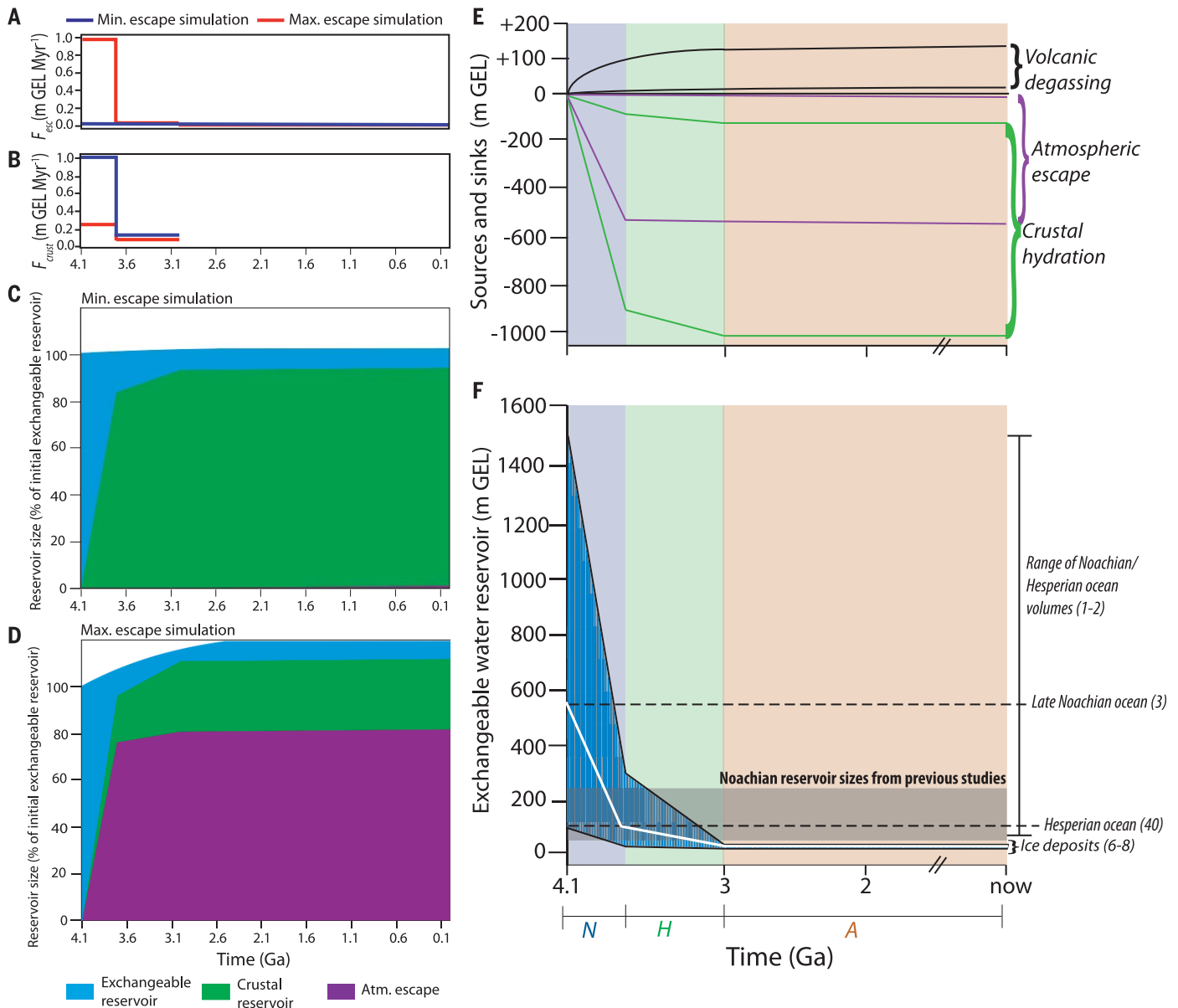
Fig. 4. Compilation of relative reservoir sizes through time from all our simulations. (**A** to **D**) Model simulations with minimum and maximum possible atmospheric escape fluxes (F_{esc}) and crustal hydration fluxes (F_{crust}) within allowed parameter space and simulation constraints, where the exchangeable reservoir D/H of 5 to 10 × SMOW must be reproduced. (A) Evolution of minimum (blue line) and maximum (red line) F_{esc} within the constrained simulation space through geological time. (B) Evolution of minimum (red line) and maximum (blue line) F_{crust} within the constrained simulation space through geological time. [(C) and (D)] Size evolution of three simulated reservoirs through geological time shown as a cumulative percentage. Colored areas indicate the time evolution within the exchangeable reservoir (blue), crustal reservoir (green), and water escaped to the atmosphere (purple). (C) The scenario in which F_{esc} is minimized and F_{crust} is maximized. (D) The scenario in which F_{esc} is maximized and F_{crust} is minimized. (**E**) Upper and lower bounds on sources and sinks from Fig. 1 through time derived from our simulations (black, volcanic degassing source; green, crustal hydration sink; purple, atmospheric escape sink) (*5*). (**F**) The range of exchangeable reservoir sizes (teal) permitted by our simulations. For comparison, we show the reservoirs derived by previous studies (gray rectangle) (*4, 11, 14, 15*) and ocean sizes based on geomorphological evidence (dashed lines) (*1–3, 40*). Our preferred simulation scenario is shown as a solid white line. Noachian (N), Hesperian (H), and Amazonian (A) time intervals used in model are shaded in blue, green, and red, respectively.

the hydration and volcanic flux magnitudes (Fig. 3C).

Crustal hydration as a water sink

Considering the simulations over our whole parameter space, we found that the amounts of water lost through crustal hydration and atmospheric escape vary in ratios ranging from 3:8 to 99:1 (Fig. 4 and figs. S4 to S6), which is equivalent to ~30 to 99% of initial water being lost through crustal hydration (*5*). The maximum proportional contribution of atmospheric escape occurs when the volume of the crustal water reservoir is minimum and vice versa. Any larger proportional escape would produce D/H heavier than the present-day observed value (>10 × SMOW). However, the absolute allowed volumes of integrated crustal hydration and atmospheric escape are dependent on the size of the initial exchangeable reservoir (figs. S4 to S6). For some of our

Table 1. Summary of parameters assumed or calculated in our preferred scenario. We list the assumed parameter values for our preferred simulation (Fig. 4F) and our reasoning for each choice. This preferred simulation reproduces a D/H composition of ~5.3 × SMOW for the present-day atmosphere and an initial exchangeable reservoir size of ~570 m GEL. Myr, million years.

Variable	Meaning	Value	Units	Reasoning
Calculated				
$R_{ex,end}$	D/H of present-day exchangeable reservoir	~5.3 × SMOW	N/A	Calculated result of our preferred model
$X_{ex,0}$	Initial size of exchangeable reservoir	~570	m GEL	Calculated result of our preferred model
Assumed				
$R_{ex,0}$	Initial D/H of exchangeable reservoir	4 × SMOW	N/A	D/H measurements of ALH84001 (13)
R_{mantle}	D/H of mantle	1.275 × SMOW	N/A	D/H measurements of meteorites (47)
$\alpha_{smectite-H_2O}$	D/H fractionation factor between smectite and water	0.95	N/A	Literary review of geochemical experiments (table S2) (5)
α_{escape}	D/H fractionation factor of atmospheric escape	0.16	N/A	Photochemical model result (29)
$X_{ex,end}$	Present-day size of exchangeable reservoir	20 to 40	m GEL	A range of remote sensing evidence (5)
$F_{crust,N}$	Rate of water drawdown by crustal hydration during the Noachian	1.25	m GEL Myr^{-1}	Intermediate value based on remote sensing evidence (5, 18)
$F_{crust,H}$	Rate of water drawdown by clay formation during the Hesperian	0.07	m GEL Myr^{-1}	Intermediate value based on remote sensing evidence (5, 18)
f_{mantle}	Water content of mantle	100	ppm	Most commonly adopted meteorite measurements (5, 24)
$F_{volcanic}$	Rate of volcanic degassing of H$_2$O	Time-dependent fluxes	m GEL Myr^{-1}	Compiled from two thermal evolution models (24)
$F_{volcanic,A}$	Rate of volcanic production after 2.5 Ga	2 × 10^{-4}	m GEL Myr^{-1}	Geological remote sensing evidence (5)
$F_{esc,A}$	Present-day H escape flux	5 × 10^{26}	H atoms s^{-1}	Spacecraft measurements (5, 16)
$F_{esc,N}$	H escape flux during the Noachian	10^{27}	H atoms s^{-1}	Modeled in this study (figs. S2 and S3) (5)
$F_{esc,H}$	H escape flux during the Hesperian	10^{27}	H atoms s^{-1}	Modeled in this study (figs. S2 and S3) (5)
t_{N-A}	End of deep, Noachian crustal alteration	3.7	Ga	Most commonly adopted age (5)
t_{H-A}	End of shallow, Hesperian crustal alteration	3.0	Ga	Most commonly adopted age (5)

model solutions, no difference in the average atmospheric escape flux relative to the present-day flux is required to account for the observed increase in D/H and decrease in the exchangeable water reservoir (Fig. 4 and figs. S3 and S4). Both the maximum and minimum escape-to-space cases (Fig. 4 and figs. S4 to S6) occur with intermediate assumed initial exchangeable reservoir volumes (~500 m GEL).

Accounting for water loss through both crustal hydration and atmospheric escape (figs. S4 to S6) resolves the apparent contradiction between the estimates of integrated H escape, the D/H of present-day Mars, and geological estimates of a large and ancient exchangeable reservoir (1, 4). These can be reconciled because the amount of atmospheric escape needed for the atmosphere to reach the present-day D/H is reduced by the removal of large initial water volumes through crustal hydration. Our models require larger Noachian exchangeable reservoirs (100 to 1500 m GEL) than those of previous work (50 to 240 m GEL) because we include crustal hydration

(Fig. 4F). The whole parameter space allows for initial exchangeable water reservoirs of 100 to 1500 m GEL at 4.1 billion years ago, 20 to 300 m GEL at the Noachian-Hesperian boundary, and a near-constant 20 to 40 m GEL throughout the Amazonian (Fig. 4F). We chose a preferred solution on the basis of observational constraints on the parameter space (Table 1 and Fig. 4F). In this preferred simulation, the Noachian and Hesperian H escape fluxes are twice that of today: $F_{esc,N} = F_{esc,H} \sim 10^{27}$ H atoms s^{-1}. The KINETICS simulations indicate that the most probable long-term H escape flux was similar to that of today, although there may have been enhancements of shorter duration, such as during dust storms or surface fluxes of H$_2$ from geologic processes (figs. S2 and S3) (5). In the preferred model, crustal hydration removes 500 m GEL and 50 m GEL during the Noachian and Hesperian, respectively, corresponding to roughly 3 wt % H$_2$O in Noachian crust of 5 km thickness and 1 wt % H$_2$O in Hesperian crust of 1 km thickness (18). This is compatible with

the range of present-day water contents and crustal reservoir depths measured from orbit and rovers (5). $F_{volcanic}$ is assumed on the basis of volcanic degassing simulations (24), which themselves assumed $f_{mantle} = 100$ ppm on the basis of meteorite measurements (5). This is compatible with observational constraints on crustal production rates and water contents of martian meteorites (5). Our preferred simulation is therefore similar to the minimum escape case shown in Fig. 4C. These simulations adopt $R_{ex,0} = 4$ × SMOW on the basis of meteorite measurements (5) and produce a present-day D/H of ~5.3 × SMOW.

Consequences for Mars evolution

If the planet accreted with 0.1 to 0.2 wt % water (32), the large Noachian exchangeable reservoirs predicted by the model are consistent with Mars primordial water volumes. A martian primordial volume of >1100 m GEL (potentially thousands of meters of GEL) could have been produced by catastrophic outgassing of the mantle (~500 to 6000 m GEL)

(33, 34), delivery of water through impacts (600 to 2700 m GEL) (35), and/or capture of gasses from the protoplanetary disc (36). However, the high hydrogen loss rates indicated by the D/H at 4.1 billion years ago recorded within meteorites (4, 11) and possible evidence for hydrodynamic escape in xenon isotopes (37) suggest that a large part of the primordial atmosphere and water were lost during the pre-Noachian period. Our proposed volumes of a 100 to 1500 m GEL during the early Noachian are within the lower end of these predicted primordial volumes and would therefore be compatible with the loss of a large part of the primordial atmosphere. After loss of the primordial atmosphere, isotope measurements of carbon and argon suggest that loss of a large fraction of these elements from the remaining martian atmosphere and the reservoirs that exchange with the atmosphere would have occurred after 4.1 billion years ago (22, 37–39). This matches our proposed trajectory of water loss within the exchangeable reservoir, which is reduced by 80 to 99% after 4.1 billion years ago within our model simulations.

Our modeled initial reservoirs are also consistent with geological estimates of Noachian and Hesperian surface water volumes. A 100 to 150-m GEL ocean during the Hesperian (1, 40) has been suggested from geomorphological observations and is compatible with our preferred simulation. A larger 550 m GEL ocean that has been suggested at the Noachian-Hesperian boundary (3) is possible in simulations in which F_{crust} and F_{esc} are both maximized in the Noachian and Hesperian, requiring the initial exchangeable water reservoir at 4.1 billion years ago to be a ~1500 m GEL (Fig. 4F). Even larger oceans of 1000 to 1500 m GEL have been proposed on the basis of geomorphology (1, 2); these would be permitted only in certain simulation scenarios during the early Noachian and not later epochs (Fig. 4F).

Our models are compatible with the major observed trajectories of the martian climate. A high-volume Noachian exchangeable reservoir is consistent with geomorphological evidence for large volumes of Noachian surface waters and observed widespread hydrated mineral formation. Aqueous alteration of the crust could have produced periods of warmer and wetter climates (supplementary text) (41–43) through accumulation of H_2 in the atmosphere (figs. S4 to S6). In cases in which atmospheric escape dominates water loss over the crustal hydration sink, H loss could be balanced by atmospheric oxygen escape (18 to 58 m GEL) and crustal oxidation (~30 to 380 m GEL) (supplementary text). However, in cases in which crustal hydration dominates water loss, short-term accumulation of H_2 could have occurred (supplementary text). In our KINETICS simulations, the accumulation of

H_2 in the atmosphere results in increased H escape flux (fig. S3) (5).

The permitted parameter space of our D/H model allows either (i) a Hesperian exchangeable reservoir that was initially large but smaller than the Noachian reservoir (≤300-m GEL) and decreased or (ii) a Hesperian reservoir that was similar to present-day levels of a 20 to 40 m GEL (Fig. 4F). In case (i), the Hesperian may have had sustained periods of warm and wet climate, which could have caused chemical weathering on a global scale and potentially formed an ocean (1, 40). In case (ii), the Hesperian climate was likely similar to the Amazonian climate, with the exception of few local and short-lived instances of surface liquid water reservoirs (44). During the Amazonian period, the low H escape flux and low volcanic degassing flux counter each other, producing low model water availability within the exchangeable reservoir that is consistent with geomorphological and mineralogical evidence of an arid climate (Fig. 4F) (31, 45).

Crustal hydration would produce a buried water reservoir with a composition reflecting that of the Noachian exchangeable reservoir of ~2 to 4 × SMOW. Martian meteorites that are 1.6 billion to 0.1 billion years old have D/H values of ~2 to 3 × SMOW (20, 21). Previously proposed explanations include a distinct subsurface fluid reservoir, mixing between low–D/H igneous and high–D/H present-day atmospheric material, or terrestrial contamination (20, 21). We suggest that exchange between younger igneous rocks and fluids derived from hydrated Noachian (~2 to 4 × SMOW) crust could account for the intermediate D/H in these meteorites.

Comparative planetary evolution

We conclude that the increasing aridity of Mars over its history was caused by the sink of chemical weathering of the crust (Fig. 4), which was recorded in the widespread Noachian hydrated minerals on the planet's surface (18). On Earth, crustal hydration also occurs, but plate tectonics enables recycling of crustal water that is eventually outgassed to the atmosphere through volcanism (46). This has facilitated sustained participation of water in the hydrologic cycle throughout geological history on Earth (46). The ancient age of most hydrated minerals (45) indicates that any such recycling did not persist on Mars. Irreversible chemical weathering therefore plays a role in regulating the habitability of terrestrial planets by controlling the time scales of sustained participation of water in the hydrologic cycle.

Our model makes testable predictions for D/H measurements of the rock and ice record (Figs. 2 and 3): a substantial long-term secular increase in D/H over the Noachian and potentially Hesperian, with little change over the Amazonian. Under a variable climate, our

model also indicates that the geological record might contain evidence of short-term D/H cyclicity: Transient warm periods with greater atmospheric H_2O (42) would periodically increase crustal hydration and escape flux, rapidly increasing D/H, whereas during cold periods, the D/H would decrease or increase slowly, depending on the balance between volcanic degassing and atmospheric escape.

REFERENCES AND NOTES

1. M. H. Carr, J. W. Head, *J. Geophys. Res. Planets* **108**, 5042 (2003).
2. S. M. Clifford, T. J. Parker, *Icarus* **154**, 40–79 (2001).
3. G. Di Achille, B. M. Hynek, *Nat. Geosci.* **3**, 459–463 (2010).
4. H. Kurokawa et al., *Earth Planet. Sci. Lett.* **394**, 179–185 (2014).
5. Materials and methods are available as supplementary materials.
6. M. T. Zuber et al., *Science* **282**, 2053–2060 (1998).
7. J. J. Plaut et al., *Science* **316**, 92–95 (2007).
8. P. R. Christensen, *Elements* **2**, 151–155 (2006).
9. T. M. Donahue, *Nature* **374**, 432–434 (1995).
10. C. R. Webster et al., *Science* **341**, 260–263 (2013).
11. G. L. Villanueva et al., *Science* **348**, 218–221 (2015).
12. N. Z. Boctor, C. M. O. D. Alexander, J. Wang, E. Hauri, *Geochim. Cosmochim. Acta* **67**, 3971–3989 (2003).
13. J. P. Greenwood, S. Itoh, N. Sakamoto, E. P. Vicenzi, H. Yurimoto, *Geophys. Res. Lett.* **35**, L05203 (2008).
14. H. Lammer et al., *Int. J. Astrobiol.* **2**, 195–202 (2003).
15. N. R. Alsaeed, B. M. Jakosky, *J. Geophys. Res. Planets* **124**, 3344–3353 (2019).
16. B. M. Jakosky et al., *Icarus* **315**, 146–157 (2018).
17. M. A. Chaffin et al., *Geophys. Res. Lett.* **41**, 314–320 (2014).
18. J. F. Mustard, Sequestration of volatiles in the Martian crust through hydrated minerals: A significant planetary reservoir of water, in *Volatiles in the Martian Crust* (Elsevier, ed. 2, 2019), pp. 247–264.
19. L. A. Leshin, *Geophys. Res. Lett.* **27**, 2017–2020 (2000).
20. T. Usui, C. M. O. D. Alexander, J. Wang, J. I. Simon, J. H. Jones, *Earth Planet. Sci. Lett.* **410**, 140–151 (2015).
21. Y. Liu et al., *Earth Planet. Sci. Lett.* **490**, 206–215 (2018).
22. R. Hu, D. M. Kass, B. L. Ehlmann, Y. L. Yung, *Nat. Commun.* **6**, 10003 (2015).
23. T. Chacko, D. R. Cole, J. Horita, *Rev. Mineral.* **43**, 1–81 (2001).
24. M. Grott, A. Morschhauser, D. Breuer, E. Hauber, *Earth Planet. Sci. Lett.* **308**, 391–400 (2011).
25. M. Allen, Y. L. Yung, J. W. Waters, *J. Geophys. Res. Space Phys.* **86**, 3617–3627 (1981).
26. H. Nair, M. Allen, A. D. Anbar, Y. L. Yung, R. T. Clancy, *Icarus* **111**, 124–150 (1994).
27. P. Gillet et al., *Earth Planet. Sci. Lett.* **203**, 431–444 (2002).
28. E. Cangi, M. S. Chaffin, J. Deighan, *J. Geophys. Res. Planets* **125**, (2020).
29. V. Krasnopolsky, *Icarus* **148**, 597–602 (2000).
30. Y. L. Yung et al., *Icarus* **76**, 146–159 (1988).
31. J. F. Kasting, J. B. Pollack, *Icarus* **53**, 479–508 (1983).
32. R. Brasser, *Space Sci. Rev.* **174**, 11–25 (2013).
33. L. T. Elkins-Tanton, *Earth Planet. Sci. Lett.* **271**, 181–191 (2008).
34. N. V. Erkaev et al., *Planet. Space Sci.* **98**, 106–119 (2014).
35. J. Lunine, J. Chambers, A. Morbidelli, L. A. Leshin, *Icarus* **165**, 1–8 (2003).
36. H. Lammer et al., *Space Sci. Rev.* **174**, 113–154 (2013).
37. B. M. Jakosky, J. H. Jones, *Rev. Geophys.* **35**, 1–16 (1997).
38. S. K. Atreya et al., *Geophys. Res. Lett.* **40**, 5605–5609 (2013).
39. B. M. Jakosky et al., *Science* **355**, 1408–1410 (2017).
40. M. H. Carr, J. Head, *Icarus* **319**, 433–443 (2019).
41. R. D. Wordsworth, *Annu. Rev. Earth Planet. Sci.* **44**, 381–408 (2016).
42. R. D. Wordsworth, L. Kerber, R. T. Pierrehumbert, F. Forget, J. W. Head, *J. Geophys. Res. Planets* **120**, 1201–1219 (2015).
43. N. J. Tosca, I. A. M. Ahmed, B. M. Tutolo, A. Ashpitel, J. A. Hurowitz, *Nat. Geosci.* **11**, 635–639 (2018).

44. J. P. Grotzinger *et al.*, *Science* **350**, aac7575 (2015).
45. B. L. Ehlmann *et al.*, *Nature* **479**, 53–60 (2011).
46. H. Lammer *et al.*, *Astron. Astrophys. Rev.* **17**, 181–249 (2009).
47. T. Usui, C. M. O. D. Alexander, J. Wang, J. I. Simon, J. H. Jones, *Earth Planet. Sci. Lett.* **357-358**, 119–129 (2012).
48. E. L. Scheller, Mars D/H model and KINETICS data files (version 1.0). CaltechDATA (2021); doi:10.22002/D1.1879.

Long-term drying of Mars by sequestration of ocean-scale volumes of water in the crust

E. L. Scheller, B. L. Ehlmann, Renyu Hu, D. J. Adams, and Y. L. Yung

Burying Mars' ancient water in the crust

Mars once had oceans of liquid water on its surface but little of that water remains today in the planet's ice caps and atmosphere. This discrepancy is usually interpreted as loss of water to space, supported by the atmospheric deuterium/hydrogen (D/H) ratio, but this has been difficult to reconcile with other constraints. Scheller *et al.* propose that water could instead have been incorporated into minerals in the planet's crust, which were later buried (see the Perspective by Kurokawa). They simulated the evolution of the D/H ratio and atmospheric loss rates for a range of plausible conditions, finding that 30 to 99% of Mars' initial water was buried in the crust.

Science, this issue p. 56; see also p. 27

View the article online
https://www.science.org/doi/10.1126/science.abc7717
Permissions
https://www.science.org/help/reprints-and-permissions

Use of this article is subject to the Terms of service